INTERNATIONAL JOURNAL FOR NUMERICAL METHODS IN FLUIDS. VOL. 13, 883–894 (1991)

SHOCK CAPTURING FOR STEADY, SUPERSONIC, TWO-DIMENSIONAL ISENTROPIC FLOW

P. GLAISTER

Department of Mathematics, PO Box 220, University of Reading, Whitcknights, Reading RG6 2AX, U.K.

SUMMARY

A finite difference scheme is presented for the solution of the two-dimensional equations of steady, supersonic, isentropic flow. The scheme incorporates numerical characteristic decomposition, is shock-capturing by design and incorporates space marching as a result of the assumption that the flow is wholly supersonic in at least one space dimension. Results are shown for problems involving oblique hydraulic jumps and reflection from a wall.

KEY WORDS Shock capturing Steady Supersonic Isentropic

1. INTRODUCTION

Some engineering applications deal with supersonic flow governed by the steady, isentropic flow equations. This is particularly true for hydraulic engineering dealing with open channels carrying supercritical flows, to which the equations of isentropic flow apply using the standard gas dynamics analogy with the shallow water equations. Typical examples are sewer systems, spillways and naturally occurring mountainous streams and rivers during heavy rainfall. It is widely accepted that the analysis and design of channels having supercritical flow can be carried out using this model.[1–10]

Of the aforementioned references, only three numerical schemes have any degree of success in computing oblique jumps. In Reference 1 Lax and MacCormack schemes are used to compute supercritical, free surface flows, although the jump is spread over a number of mesh points. A shock-tracking scheme was used by Pandolfi,[3] whilst Demuren[4] adapted the numerical methods of Patankar and Spalding for the calculation of supercritical, free surface flows in open channels.

In 1988 Glaister[11] presented a numerical scheme for the one-dimensional, unsteady Euler equations with general equations of state. This scheme (i) captures shocks automatically over two or three cells, (ii) is second-order-accurate and (iii) is computationally efficient. It is the underlying ideas of this scheme that we use in this paper to develop a new scheme for steady, supersonic, isentropic flows. Importantly, the scheme is also efficient, second-order-accurate and captures oblique shocks over two or three cells. As mentioned previously, we apply space marching by observing that the resulting equations are hyperbolic with respect to one marching direction. The scheme is then applied to two problems concerning oblique standing waves governed by the steady shallow water equations by employing the gas dynamics analogy mentioned above.

0271–2091/91/170883–12$06.00

Received September 1990
Revised December 1990

2. GOVERNING EQUATIONS

The equations governing the isentropic flow of gas in a pipe of rectangular cross-section can be written in conservation form as

$$\mathbf{w}_t + \mathbf{F}_x + \mathbf{G}_y = \mathbf{0}, \tag{1}$$

where

$$\mathbf{w} = (\rho, \rho u, \rho v)^{\mathrm{T}}, \tag{2a}$$

$$\mathbf{F}(\mathbf{w}) = (\rho u, \rho u^2 + p, \rho uv)^{\mathrm{T}}, \tag{2b}$$

$$\mathbf{G}(\mathbf{w}) = (\rho v, \rho uv, \rho v^2 + p), \tag{2c}$$

$$p = p(\rho). \tag{3}$$

Equation (3) is a known gas law. The quantities $\rho = \rho(x, y, t)$ and $u = u(x, y, t)$, $v = v(x, y, t)$ represent the density and the components of the fluid velocity in the x- and y-directions respectively at a general position x, y and at time t. Equations (1)–(3) represent conservation of mass and momentum.

In this paper it is the steady form of equation (1) that we consider. Thus with $\mathbf{w}_t = \mathbf{0}$ and $(\rho, u, v, p) = (\rho, u, v, p)(x, y)$ we have

$$\mathbf{F}_x + \mathbf{G}_y = \mathbf{0}, \tag{4a}$$

with $\mathbf{F}$ and $\mathbf{G}$ as before, together with a boundary condition

$$\mathbf{w}(x_0, y) = \mathbf{w}_0(y). \tag{4b}$$

3. SPACE MARCHING

Consider solving (4a, b) with $\mathbf{F}$ and $\mathbf{G}$ as defined by (2b, c), which can be written as

$$\mathbf{F}_x + \mathbf{A}\mathbf{F}_y = \mathbf{0}. \tag{5}$$

If the Jacobian $\mathbf{A} = \partial\mathbf{G}/\partial\mathbf{F}$ has real, distinct eigenvalues, then the system (4a) is hyperbolic and we shall assume this to be the case here. This assumption corresponds to the flow governed by (4a, b) being supersonic everywhere. Thus it is appropriate to use techniques similar to those developed for time-dependent conservation laws of the form

$$\mathbf{c}_t + \mathbf{H}(\mathbf{c})_x = \mathbf{0}, \qquad \mathbf{c}(x, 0) = \mathbf{c}_0(x), \tag{6}$$

i.e.

$$\mathbf{c}_t + \mathbf{E}\mathbf{c}_x = \mathbf{0}, \tag{7}$$

where $\mathbf{c}$ is the conserved variable and $\mathbf{E} = \partial\mathbf{H}/\partial\mathbf{c}$. Instead of marching forward in time 't', for (4a, b) we march forward in the space variable 'x', for example. In particular, smooth solutions of (6) will develop discontinuities (shock) in time and likewise (4a, b) will exhibit oblique jumps in space.

A specific technique for solving (6) in the case of the unsteady Euler equations with real gases was given in Reference 11 and we develop similar ideas here for solving (4a, b). The scheme in Reference 11 represents an approximation to the scheme of Godunov,[12] and the scheme presented here can be viewed in a similar way. Although we use the concept of a Riemann problem as in Reference 11 by identifying 'x' as a timelike variable, three important differences remain. Firstly, the structure differs as a result of the equations of flow being different, and the

resulting construction of the scheme is more detailed, although its actual implementation is just as straightforward; secondly, the scheme applies only to flows that are wholly supersonic in at least one direction, which we take, without loss of generality, to be the x-direction; and finally, the flow is assumed to be steady. Thus it is imperative that the x-axis is aligned with one of these directions, e.g. the predominant flow direction.

4. LINEARIZED RIEMANN PROBLEM

If an approximate solution of equations (4a, b) is sought (along a y-co-ordinate line $x=x_j$) using a finite difference method, then the solution is known at a set of discrete mesh points $(x, y)=(x_j, y_k)$. The approximate solution $\mathbf{w}_k^j$ to $\mathbf{w}$ at (x_j, y_k) can be considered as a set of piecewise constants $\mathbf{w}=\mathbf{w}_k^j$ for $y\in(y_k-\Delta y/2,\ y_k+\Delta y/2)$, where $\Delta y=y_k-y_{k-1}$ is a constant mesh spacing (see e.g. Reference 12). A Riemann problem is now present at each interface $y_{k-1/2}=\frac{1}{2}(y_{k-1}+y_k)$ separating adjacent states $\mathbf{w}_{k-1}^j$ and $\mathbf{w}_k^j$. If the steady equations (4a, b) are linearized by considering the Jacobian matrix $\mathbf{A}=\partial\mathbf{G}/\partial\mathbf{F}$ to be constant in each interval (y_{k-1}, y_k), say $\tilde{\mathbf{A}}=\tilde{\mathbf{A}}(\mathbf{w}_{k-1}^j, \mathbf{w}_k^j)$, then the resulting equations

$$\mathbf{F}_x+\tilde{\mathbf{A}}\mathbf{F}_y=\mathbf{0} \tag{8}$$

can be solved approximately using explicit space marching in the x-direction. The step Δx is restricted so that the solutions of adjacent Riemann problems do not interact, and this sets a restriction on the mesh spacing in the x-direction once Δy has been chosen. The scalar problems that result from this analysis can be solved by upwind differencing consistent with the theory of characteristics; however, an approximate Jacobian matrix needs to be constructed in each interval so that jumps can be captured automatically. Thus, given the boundary condition $\mathbf{w}(x_0, y_k)=\mathbf{w}_0(y_k)=\mathbf{w}_k^0$, a mesh y_k in the y-direction and flow that is wholly supersonic in the x-direction, it is possible to compute in turn the approximate solution along $x=x_0+\Delta x$, $x=x_0+2\Delta x, \ldots$.

5. NUMERICAL SCHEME

Consider equations (4a, b) and begin by noting the structure associated with equations (4a) and (5).

5.1. *Structure*

Let $\mathbf{B}=\partial\mathbf{F}/\partial\mathbf{w}$ and $\mathbf{C}=\partial\mathbf{G}/\partial\mathbf{w}$ denote the Jacobians of the flux functions $\mathbf{F}$ and $\mathbf{G}$, so that the Jacobian $\mathbf{A}=\partial\mathbf{G}/\partial\mathbf{F}=\mathbf{C}\mathbf{B}^{-1}$. Denote also the eigenvalues and eigenvectors of $\mathbf{A}$ by λ_i and $\mathbf{r}_i$, $i=1, 2, 3$, respectively, so that

$$\mathbf{A}\mathbf{r}_i=\lambda_i\mathbf{r}_i, \quad i=1, 2, 3, \tag{9}$$

and hence

$$(\mathbf{C}-\lambda_i\mathbf{B})\mathbf{e}_i=\mathbf{0}, \qquad i=1, 2, 3, \tag{10}$$

where

$$\mathbf{B}\mathbf{e}_i=\mathbf{r}_i, \qquad i=1, 2, 3. \tag{11}$$

Another associated matrix is $\mathscr{A}=\mathbf{B}^{-1}\mathbf{C}$ since (4a) can be written as

$$\mathbf{w}_x+\mathscr{A}\mathbf{w}_y=\mathbf{0}, \tag{12}$$

and from (10)

$$(\mathbf{B}^{-1}\mathbf{C}-\lambda_i\mathbf{I})\mathbf{e}_i=\mathbf{0}. \quad i=1, 2, 3, \tag{13}$$

so that $\mathscr{A}$ has eigenvalues λ_i with eigenvectors $\mathbf{e}_i$. In the Appendix we state **A**, $\mathscr{A}$, **B** and **C**. Solving (10), we find that

$$\lambda_{1,2,3}=\frac{uv\pm a^2\sqrt{(M^2-1)}}{u^2-a^2}, \quad \frac{v}{u}, \tag{14a–c}$$

$$\mathbf{e}_{1,2}=\left(\frac{v}{\sqrt{(M^2-1)}}\pm u, \pm(u^2-a^2), a^2\sqrt{(M^2-1)}\pm uv\right)^{\mathrm{T}}, \tag{15a, b}$$

$$\mathbf{e}_3=(0, u, v)^{\mathrm{T}}, \tag{15c}$$

where M is the local Mach number given by

$$M^2=\frac{u^2+v^2}{a^2}, \tag{16}$$

which is assumed to satisfy $M>1$, and a is the local sound speed given by

$$a^2=\frac{\mathrm{d}p}{\mathrm{d}\rho}, \tag{17}$$

using the gas law (3).

5.2. *Construction of* $\tilde{\mathbf{A}}$

In constructing numerical solutions to (4a) or (5), it is our aim, as stated in Section 4, to obtain an approximation to the Jacobian $\mathbf{A}=\partial\mathbf{G}/\partial\mathbf{F}$ in an interval (y_{k-1}, y_k), so that approximate solutions can be sought to the linearized Riemann problem (8).

Consider two adjacent states $\mathbf{w}_{k-1}^j=\mathbf{w}_{\mathrm{L}}$ and $\mathbf{w}_k^j=\mathbf{w}_{\mathrm{R}}$ (left and right) given at either end of the cell $(y_{k-1}, y_k)=(y_{\mathrm{L}}, y_{\mathrm{R}})$ on the x-co-ordinate line $x=x_j$. Following the analogy of the steady problem (5) with the unsteady problem (7) made in Section 3, and the work in Reference 11, it is appropriate to construct the approximate Jacobian $\tilde{\mathbf{A}}=\tilde{\mathbf{A}}(\mathbf{w}_{\mathrm{L}}, \mathbf{w}_{\mathrm{R}})$ in this cell such that

$$\tilde{\mathbf{A}}\Delta\mathbf{F}=\Delta\mathbf{G} \tag{18}$$

for all jumps $\Delta\mathbf{F}$, where $\Delta(\cdot)=(\cdot)_{\mathrm{R}}-(\cdot)_{\mathrm{L}}$. This will mean that oblique jumps will be captured automatically. The matrix $\tilde{\mathbf{A}}$ is assumed to have the form of **A** with the flow variables a, u and v replaced by averages $\tilde{a}$, $\tilde{u}$ and $\tilde{v}$ over the cell $(y_{\mathrm{L}}, y_{\mathrm{R}})$, and these averages are determined by solving (18).

Equivalently we could seek matrices $\tilde{\mathbf{B}}$ and $\tilde{\mathbf{C}}$ (see Appendix) such that

$$\tilde{\mathbf{B}}\Delta\mathbf{w}=\Delta\mathbf{F} \quad \text{and} \quad \tilde{\mathbf{C}}\Delta\mathbf{w}=\Delta\mathbf{G} \tag{19a, b}$$

for any jump $\Delta\mathbf{w}$, and hence by combining (18) and (19a, b),

$$\tilde{\mathbf{A}}=\tilde{\mathbf{C}}\tilde{\mathbf{B}}^{-1}. \tag{20}$$

Denoting the eigenvalues of $\tilde{\mathbf{A}}$ by $\tilde{\lambda}_i$ with corresponding eigenvectors $\tilde{\mathbf{r}}_i$, then similar relationships to those in Section 5.1 hold, i.e. $\tilde{\mathscr{A}}$ has eigenvalues $\tilde{\lambda}_i$ with eigenvectors $\tilde{\mathbf{e}}_i$, where

$$(\tilde{\mathbf{C}}-\tilde{\lambda}_i\tilde{\mathbf{B}})\tilde{\mathbf{e}}_i=\mathbf{0}, \quad i=1, 2, 3, \tag{21}$$

$$\tilde{\mathbf{B}}\mathbf{e}_i=\tilde{\mathbf{r}}_i, \quad i=1, 2, 3. \tag{22}$$

Solving (21) gives

$$\tilde{\lambda}_{1,2,3}=\frac{\tilde{u}\tilde{v}\pm\tilde{a}^2\sqrt{(\tilde{M}^2-1)}}{\tilde{u}^2-\tilde{a}^2},\quad \frac{\tilde{v}}{\tilde{u}}, \tag{23a–c}$$

$$\tilde{\mathbf{e}}_{1,2}=\left(\frac{\tilde{v}}{\sqrt{(\tilde{M}^2-1)}}\pm\tilde{u},\ \pm(\tilde{u}^2-\tilde{a}^2),\ \tilde{a}^2\sqrt{(\tilde{M}^2-1)}\pm\tilde{u}\tilde{v}\right)^{\mathrm{T}}, \tag{24a, b}$$

$$\tilde{\mathbf{e}}_3=(0,\tilde{u},\tilde{v})^{\mathrm{T}}, \tag{24c}$$

where

$$\tilde{M}^2=\frac{\tilde{u}^2+\tilde{v}^2}{\tilde{a}^2} \tag{25}$$

and the averages $\tilde{a}$, $\tilde{u}$ and $\tilde{v}$ are still to be determined. Before giving the solution to this problem, we write down the numerical scheme for (4a, b) and from this it will be evident which information we shall require.

5.3. *Numerical scheme*

We propose solving (4a, b) via approximate Riemann solutions of

$$\mathbf{w}_x+\tilde{\mathscr{A}}\mathbf{w}_y=\mathbf{0}, \tag{26}$$

where $\tilde{\mathscr{A}}=\tilde{\mathbf{B}}^{-1}\tilde{\mathbf{C}}$ (compare with (12)). This gives rise to the upwinded scheme

$$\frac{\mathbf{w}_l^{j+1}-\mathbf{w}_l^j}{\Delta x}+\tilde{\mathscr{A}}\,\frac{\mathbf{w}_k^j-\mathbf{w}_{k-1}^j}{\Delta y}=\mathbf{0}, \tag{27}$$

where l can be $k-1$ or k. By projecting

$$\Delta\mathbf{w}=\mathbf{w}_k^j-\mathbf{w}_{k-1}^j=\mathbf{w}_{\mathrm{R}}-\mathbf{w}_{\mathrm{L}}=\sum_{i=1}^{3}\tilde{\alpha}_i\tilde{\mathbf{e}}_i, \tag{28}$$

(27) gives, in view of (21),

$$\frac{\mathbf{w}_l^{j+1}-\mathbf{w}_l^j}{\Delta x}+\frac{\sum_{i=1}^{3}\tilde{\lambda}_i\tilde{\alpha}_i\tilde{\mathbf{e}}_i}{\Delta y}=\mathbf{0} \tag{29}$$

along a y-co-ordinate line $x=x_j$, where Δx and Δy represent the mesh spacing in the x- and y-directions respectively. Upwind differencing now applied to equation (29) gives the following first-order algorithm for the solution of equations (4a, b):

$$\text{add } -\frac{\Delta x}{\Delta y}\tilde{\lambda}_i\tilde{\alpha}_i\tilde{\mathbf{e}}_i \text{ to } \mathbf{w}_{\mathrm{R}} \text{ when } \tilde{\lambda}_i>0$$

or

$$\text{add } -\frac{\Delta x}{\Delta y}\tilde{\lambda}_i\tilde{\alpha}_i\tilde{\mathbf{e}}_i \text{ to } \mathbf{w}_{\mathrm{L}} \text{ when } \tilde{\lambda}_i<0. \tag{30}$$

Equivalently, by projecting

$$\Delta\mathbf{w}_{k-1/2}=\mathbf{w}_k^j-\mathbf{w}_{k-1}^j=\mathbf{w}_{\mathrm{R}}-\mathbf{w}_{\mathrm{L}}=\left(\sum_{i=1}^{3}\tilde{\alpha}_i\tilde{\mathbf{e}}_i\right)_{k-1/2}, \tag{31}$$

we split

$$\mathscr{A}\Delta\mathbf{w}_{k-1/2}=\left(\sum_{i=1}^{3}\tilde{\lambda}_i\tilde{\alpha}_i\tilde{\mathbf{e}}_i\right)_{k-1/2}=\Delta^{+}_{k-1/2}+\Delta^{-}_{k-1/2} \tag{32}$$

into contributions $\Delta^{\pm}$ from left and right travelling waves, where the $+(-)$ portion is contributed by the sum over all positive (all negative) eigenvalues. Upwind differencing is now effected by

$$\mathbf{w}_k^{j+1}=\mathbf{w}_k^{j}-\frac{\Delta x}{\Delta y}(\Delta^{+}_{k-1/2}+\Delta^{-}_{k+1/2}). \tag{33}$$

Thus we note the direction of flow of information given by the approximate eigenvalues $\tilde{\lambda}_i$ and use this information to update the solution consistent with the theory of characteristics of equation (5a). In addition, second-order transfers of these first-order increments can be made to achieve higher accuracy, provided that they are limited to maintain monotonicity.[13] The use of these 'flux limiters' improves accuracy without introducing non-physical spurious oscillations, especially at jumps.

Solving (28) gives

$$\tilde{\alpha}_{1,2}=\frac{\pm\tilde{v}-\tilde{u}[\sqrt{(\tilde{M}^2-1)}][\pm\tilde{a}^2\sqrt{(\tilde{M}^2-1)}\Delta\rho+\tilde{u}\Delta(\rho v)-\tilde{v}\Delta(\rho u)]}{2\tilde{a}^2\tilde{M}^2(\tilde{u}^2-\tilde{a}^2)}, \tag{34a, b}$$

$$\tilde{\alpha}_3=\frac{\tilde{u}\Delta(\rho u)+\tilde{v}\Delta(\rho v)-\tilde{a}^2(\tilde{M}^2-1)\Delta\rho}{\tilde{a}^2\tilde{M}^2}. \tag{34c}$$

Therefore all that remains is to determine the averages $\tilde{a}$, $\tilde{u}$ and $\tilde{v}$ to incorporate into the scheme (30), utilizing the eigenvalues $\tilde{\lambda}_i$ and eigenvectors $\tilde{\mathbf{e}}_i$ of the approximate Jacobian $\tilde{\mathscr{A}}$ and the 'wave strengths' $\tilde{\alpha}_i$ in (34a–c).

5.4. *Averages*

Using the form for $\tilde{\mathbf{A}}$ in the Appendix (or $\tilde{\mathbf{B}}$ and $\tilde{\mathbf{C}}$) and solving (18) (or (19a, b)), we obtain the following averages for $\tilde{a}$, $\tilde{u}$ and $\tilde{v}$ in (y_L, y_R) (see Appendix):

$$\tilde{u}=\frac{\sqrt{(\rho_L)}u_L+\sqrt{(\rho_R)}u_R}{\sqrt{\rho_L}+\sqrt{\rho_R}}, \tag{35a}$$

$$\tilde{v}=\frac{\sqrt{(\rho_L)}v_L+\sqrt{(\rho_R)}v_R}{\sqrt{\rho_L}+\sqrt{\rho_R}}, \tag{35b}$$

$$\tilde{a}^2=\begin{cases}\dfrac{\Delta p}{\Delta\rho} & \text{if } \Delta\rho\neq 0,\\[2ex] \dfrac{\mathrm{d}p(\rho)}{\mathrm{d}\rho} & \text{if } \Delta\rho=0, \text{ i.e. } \rho_L=\rho_R=\rho.\end{cases} \tag{36}$$

With these averages it is possible to rewrite the $\tilde{\alpha}_i$ in (34a–c) purely in terms of primitive variables ρ, u, v and p by noticing that $\Delta(\rho u)=\hat{\rho}\Delta u+\tilde{u}\Delta\rho$, where $\hat{\rho}=\sqrt{(\rho_L\rho_R)}$, and similarly for $\Delta(\rho v)$.

Thus the numerical scheme for the solution of (4a, b) is given by the marching procedure outlined in Section 3 together with the algorithm given by (30) (modified to give second-order accuracy) using the expressions in (23a)–(25) and (34a)–(36). As a result of using numerical characteristic decomposition, this scheme closely models the physics of the problem, and in particular captures oblique shocks well.

Finally, we observe that as $\Delta \mathbf{w} \to \mathbf{0}$,

$$(\tilde{\mathbf{A}}, \tilde{\mathscr{A}}, \tilde{\mathbf{B}}, \tilde{\mathbf{C}}, \tilde{\lambda}_i, \tilde{\mathbf{e}}_i, \tilde{\mathbf{r}}_i, \tilde{a}, \tilde{u}, \tilde{v}) \to (\mathbf{A}, \mathscr{A}, \mathbf{B}, \mathbf{C}, \lambda_i, \mathbf{e}_i, \mathbf{r}_i, a, u, v),$$

consistent with the continuous case.

6. TEST PROBLEM AND NUMERICAL RESULTS

In this section we present results for the solution of two test problems using the second-order scheme of Section 5 (with the superbee limiter[13]) applied to supercritical, free surface flow governed by the steady form of the shallow water equations. We are able to use the scheme here since the shallow water equations are analogous to those for isentropic flow. This analogy is completed by identifying ρ as the total height above the bottom of a channel multiplied by the acceleration due to gravity, and specifying the 'gas' law (3) as

$$p = \tfrac{1}{2}\rho^2. \tag{37}$$

(N.B. We have non-dimensionalized the standard equation $\bar{p} = \frac{1}{2} g \bar{\rho}^2$ representing this analogy, where g is the acceleration due to gravity.) The average for $\tilde{a}$ in (33) then simplifies to

$$\tilde{a}^2 = \tfrac{1}{2}(\rho_L + \rho_R). \tag{38}$$

The first problem concerns an oblique hydraulic jump or oblique standing wave, which is produced when a vertical boundary is deflected inwards to the flow as in the case of a channel contraction. This causes an abrupt depth increase which is propagated from the point of deflection in the wall to the interior of the flow field at an angle β, say, with respect to the flow direction. If the bottom friction and slope of the channel are neglected, then this problem has an analytical solution given by

$$\frac{\rho_1}{\rho_0} = \frac{\tan\beta}{\tan(\beta - \theta)}, \tag{39a}$$

$$\sin\beta = \frac{1}{M_0}\sqrt{\left[\frac{\rho_1}{2\rho_0}\left(1 + \frac{\rho_1}{\rho_0}\right)\right]}. \tag{39b}$$

In (39a, b), β represents the angle of the oblique jump with respect to the upstream flow direction, θ represents the angle of wall deflection and ρ_1 represents the value of ρ downstream of the contraction. Also, ρ_0 and M_0 denote the upstream values of ρ and M, where $V_0^2 = u_0^2 + v_0^2$, and $u_0 = V_0 \cos\theta$ and $v_0 = -V_0 \sin\theta$ denote the x- and y-components of the velocity of the upstream flow. (M now refers to the local Froude number.) Equations (39a, b) need to be solved iteratively for the ratio ρ_1/ρ_0.

For the computation presented here we align the x-axis with the wall downstream of the deflection point. We apply boundary conditions along $x = 0$ given by the upstream flow values (ρ_0, u_0, v_0) and apply reflecting boundary conditions along the wall $y = 0$ as described in Reference 11. The example chosen corresponds to an upstream flow with a Froude number $M_0 = V_0/\sqrt{\rho_0} = 4$ and a wall deflection $\theta = 12°$. The analytical solution given by (39a, b) yields $\rho_1/\rho_0 = 1{\cdot}987$ and $\beta = 25{\cdot}505°$. The numerical computation of this problem using 60 points in the x-direction and 20 points in the y-direction has resulted in the three-dimensional plot of ρ/ρ_0 shown in Figure 1. A similar calculation with 120 points in the x-direction and 40 points in the y-direction is shown in Figure 2. As stated, friction and bottom slope terms have been neglected in order to make a comparison with an analytic solution. Within the resolution of the grid, the numerical solution agrees with the analytic solution and thus no advantage is gained by

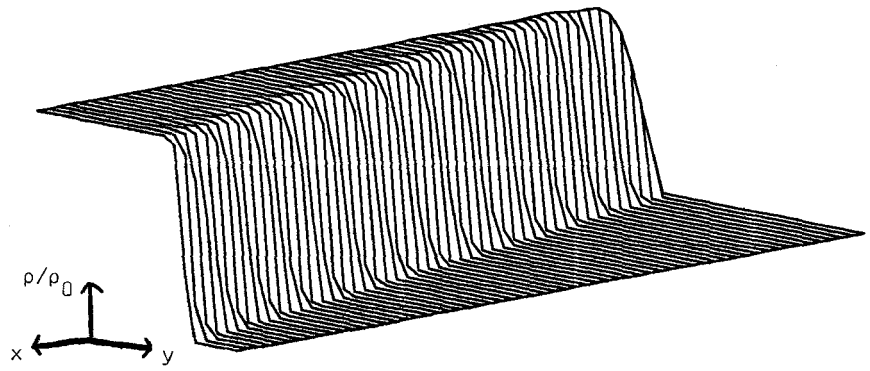

Figure 1. Plot of ρ/ρ_0 for Problem 1 with a 60×20 mesh

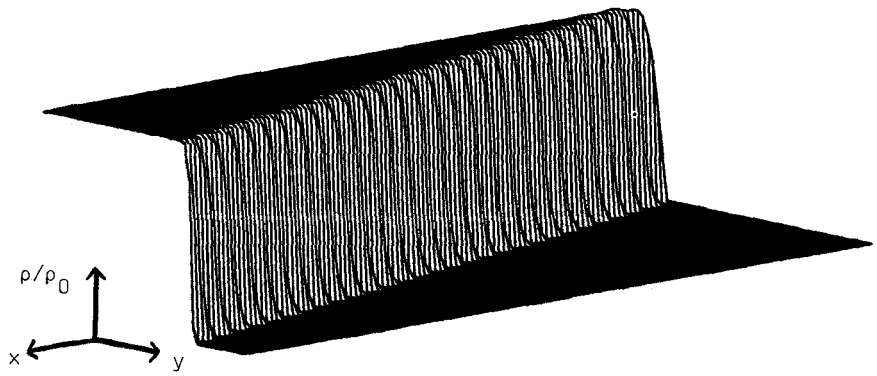

Figure 2. Plot of ρ/ρ_0 for Problem 1 with a 120×40 mesh

overplotting the exact solution. The predicted values of ρ_1, M_1 and β agree with the exact solution to three-significant-figure accuracy. In particular, the oblique jump has been captured over at most three cells; mostly over one or two.

Furthermore, the algorithm is computationally efficient. Using an Amdahl V7 and 120×40 mesh points takes 0·5 CPU seconds to compute the results in Figure 2.

The second test problem concerns an oblique hydraulic jump reflecting from a wall. In this problem a flow with $\rho = \rho_0$ and $M = M_0$ is deflected an angle θ by a turning wall. This creates an oblique jump that travels until it impinges on a wall (parallel to the initial flow), where it is reflected. We take the values $\rho_0 = 9{\cdot}800$ and $\theta = 6{\cdot}346°$, for which the oblique jump makes an angle 20·000° with the initial flow direction, and after reflection makes an angle 17·812° with the initial flow direction. The parameters downstream of the oblique jump are ρ_1 and M_1, and downstream of the reflected oblique jump are ρ_2 and M_2, where $\rho_1/\rho_0 = 1{\cdot}498$, $\rho_2/\rho_0 = 2{\cdot}092$, $M_1 = 3{\cdot}160$ and $M_2 = 2{\cdot}563$. The result of the numerical computation of this problem using the scheme of Section 5 is shown by three-dimensional plots of ρ/ρ_0 from two viewpoints in Figures 3 and 4, and with a grid comprising 60×10 mesh points takes 0·25 CPU seconds to run. A similar calculation with 120×20 points is shown in Figures 5 and 6. As for the first test problem, within the resolution of the grid the numerical solution agrees with the analytic solution and no

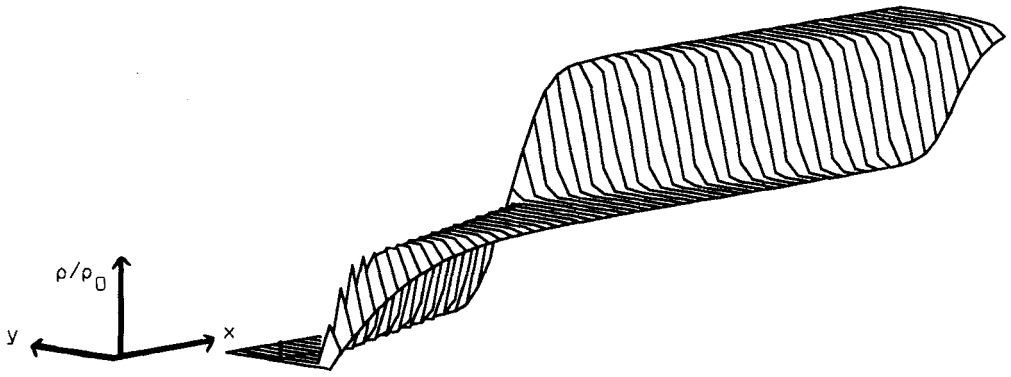

Figure 3. Plot of ρ/ρ_0 for Problem 2 with a 60×10 mesh

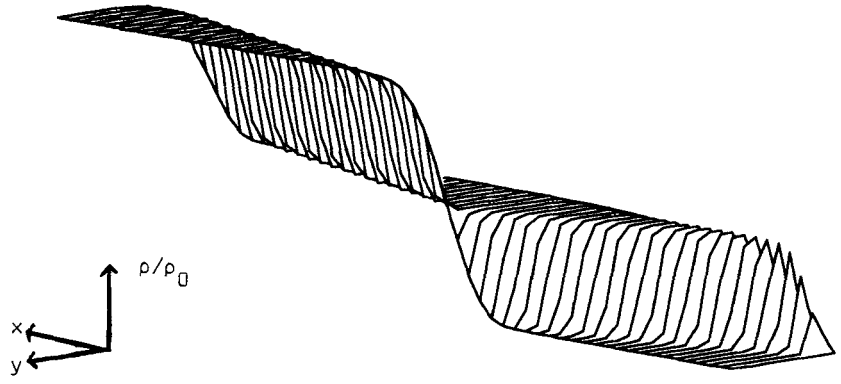

Figure 4. Plot of ρ/ρ_0 for Problem 2 with a 60×10 mesh

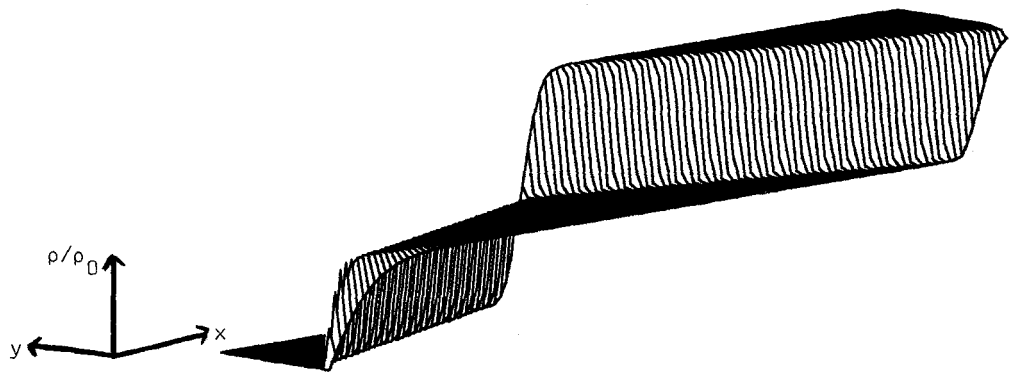

Figure 5. Plot of ρ/ρ_0 for Problem 2 with a 120×20 mesh

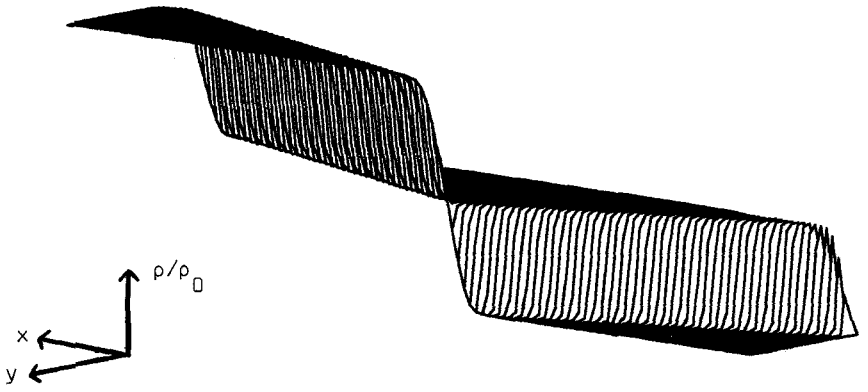

Figure 6. Plot of ρ/ρ_0 for Problem 2 with a 120×20 mesh

advantage is gained by overplotting the exact solution. The predicted values of ρ_1, ρ_2, M_1, M_2 and the shock angles agree with the exact solution to three-significant-figure accuracy.

We note that for the shallow water equations it is a straightforward matter to incorporate source terms due to friction and a non-zero bottom slope as a minor modification to the algorithm.

7. CONCLUSIONS

We have presented a numerical scheme for the equations of steady, supersonic, isentropic flow. The resulting algorithm was shown to be computationally efficient and on two test problems the numerical solution agrees with the analytic solution. In particular, the resulting oblique jumps are captured over two or three cells.

APPENDIX

We state here the Jacobians **A**, **B**, **C** and $\mathscr{A}$ their corresponding approximations and derive the averages given in Section 5.4.

Jacobians

The required Jacobians are

$$\mathbf{A}=\frac{1}{u(u^2-a^2)}\begin{bmatrix} v(u^2+a^2) & -uv & u^2-a^2 \\ 0 & 0 & u(u^2-a^2) \\ 2a^2(u^2+v^2) & -u(a^2+v^2) & 2v(u^2-a^2) \end{bmatrix}, \tag{40, 44}$$

$$\mathbf{B}=\begin{bmatrix} 0 & 1 & 0 \\ a^2-u^2 & 2u & 0 \\ -uv & v & u \end{bmatrix}, \tag{41, 45}$$

$$\mathbf{C}=\begin{bmatrix} 0 & 0 & 1 \\ -uv & v & u \\ a^2-v^2 & 0 & 2v \end{bmatrix}, \tag{42, 46}$$

$$\mathscr{A}=\frac{1}{u(u^2-a^2)}\begin{bmatrix} u^2v & -uv & u^2 \\ 0 & 0 & u(u^2-a^2) \\ a^2(u^2+v^2-a^2) & -uv^2 & v(2u^2-a^2) \end{bmatrix}, \tag{43, 47}$$

together with their corresponding approximations $\tilde{\mathbf{A}}$, $\tilde{\mathbf{B}}$, $\tilde{\mathbf{C}}$ and $\tilde{\mathscr{A}}$ given by (44)–(47) respectively, where $\tilde{u}$, $\tilde{v}$ and $\tilde{a}$ have replaced u, v and a in (40)–(43).

Averages

The averages required in Section 5 are determined by solving

$$\Delta\mathbf{G}=\tilde{\mathbf{A}}\Delta\mathbf{F} \tag{48}$$

for arbitrary jumps $\Delta\mathbf{F}$. Alternatively, we solve

$$\Delta\mathbf{F}=\tilde{\mathbf{B}}\Delta\mathbf{w} \tag{49}$$

and

$$\Delta\mathbf{G}=\tilde{\mathbf{C}}\Delta\mathbf{w} \tag{50}$$

for arbitrary jumps $\Delta\mathbf{w}$, so that $\tilde{\mathbf{A}}=\tilde{\mathbf{C}}\tilde{\mathbf{B}}^{-1}$. To achieve this, we introduce the averages

$$\hat{\rho}=\sqrt{(\rho_L\rho_R)}, \tag{51}$$

$$\hat{q}=\frac{\sqrt{(\rho_L)}q_L+\sqrt{(\rho_R)}q_R}{\sqrt{\rho_L}+\sqrt{\rho_R}}, \quad q=u, v, \tag{52}$$

from which we can show that

$$\Delta(pq)=\hat{\rho}\Delta q+\hat{q}\Delta\rho, \quad q=u, v, \tag{53}$$

$$\Delta(\rho qr)=\hat{\rho}\hat{q}\Delta r+\hat{\rho}\hat{r}\Delta q+\hat{q}\hat{r}\Delta\rho, \quad q=u, v, \quad r=u, v. \tag{54}$$

Taking equation (49) first, using the form for $\tilde{\mathbf{B}}$ from (45) and expanding using (51)–(54), we arrive at the pair of equations

$$(\tilde{u}-\hat{u})^2\Delta\rho+2\hat{\rho}(\tilde{u}-\hat{u})\Delta u+\tilde{a}^2\Delta\rho-\Delta p=0, \tag{55}$$

$$(\tilde{u}-\hat{u})(\tilde{v}-\tilde{v})\Delta\rho+\hat{\rho}(\tilde{v}-\hat{v})\Delta u+\hat{\rho}(\tilde{u}-\hat{u})\Delta v=0, \tag{56}$$

to be satisfied for all independent variations $\Delta\rho$, Δu and Δv. Equation (56) gives rise to the set of equations

$$\hat{\rho}(\tilde{u}-\hat{u})=0, \tag{57}$$

$$\hat{\rho}(\tilde{v}-\hat{v})=0, \tag{58}$$

$$(\tilde{u}-\hat{u})(\hat{v}-\tilde{v})=0, \tag{59}$$

whose systematic solution gives rise to the only physical solution ($\hat{\rho}\neq 0$), $\tilde{u}=\hat{u}$ and $\tilde{v}=\hat{v}$. Substituting this solution into (55) then gives

$$\tilde{a}^2\Delta\rho-\Delta p=0, \tag{60}$$

whose solution for $\Delta\rho \neq 0$ is

$$\tilde{a}^2 = \frac{\Delta p}{\Delta \rho}. \tag{61}$$

If $\Delta\rho = 0$, (60) is automatically satisfied and any consistent choice for $\tilde{a}^2$ will suffice, for which we set

$$\tilde{a}^2 = \frac{\mathrm{d}p}{\mathrm{d}\rho}, \tag{62}$$

giving the averages in Section 5.4. It is then a trivial matter to check that (50) is satisfied using these averages and the form for $\tilde{\mathbf{C}}$ from (46).

REFERENCES

1. O. F. Jiménez and M. H. Chaudhry, 'Computation of supercritical free-surface flows', *J. Hydraul. Eng.*, **114,** 377–395 (1988).
2. J. A. Liggett and S. U. Vasudev, 'Slope and friction effects in two dimensional, high speed flow', *Proc. 11th Int. Congr. IAHR, Vol. 1*, Leningrad, 1965, International Association for Hydraulic Research, Delft, pp. 1–12.
3. M. Pandolfi, 'Numerical experiments on free surface water motion with bores', *Proc. 4th Int. Conf. on Numerical Methods in Fluid Dynamics, Lecture Notes in Physics, Vol. 35*, Springer, New York, 1975, pp. 304–312.
4. A. O. Demuren, 'Prediction of steady surface-layer flows', *D. Phil. Thesis* (partial), University of London, 1979.
5. R. Rajar and M. Cetina, 'Two-dimensional dam-break flow in steep curved channels', *Proc. 20th Congr. IAHR, Vol. II*, Moscow, 1983, International Association for Hydraulic Research, Delft, pp. 571–579.
6. G. Bagge and J. B. Herbich, 'Transitions in supercritical open-channel flow', *J. Hydraul. Div., ASCE*, **93,** (5), 23–41 (1967).
7. J. B. Herbich and P. Walsh, 'Supercritical flow in rectangular expansions', *J. Hydraul. Div., ASCE*, **98,** (9), 1691–1700 (1972).
8. F. Villegas, 'Design of the Punchiná Spillway', *Water Power Dam Construct.*, **28,** (11), 32–34 (1976).
9. S. Dakshinamoorthy, 'High velocity flow through expansions', *Proc. 17th Congr. IAHR, Vol. 2*, Baden-Baden, 1977, International Association for Hydraulic Research, Delft, pp. 373–381.
10. J. Ilis and G. Pender, 'Chute spillway design calculations', *Proc. Inst. Civil Eng.*, **73,** (2), 299–312 (1982).
11. P. Glaister, 'An approximate linearised Riemann solver for real gases', *J. Comput. Phys.*, **74,** 382–408 (1988).
12. S. K. Godunov, 'A finite difference method for the numerical computation and discontinuous solutions of the equations of fluid dynamics', *Mat. Sborn.*, **47,** 271 (1959).
13. P. K. Sweby, 'High resolution schemes using flux limiters for hyperbolic conservation laws', *SIAM J. Numer. Anal.*, **21,** 995–1011 (1984).